HHS Public Access

Author manuscript

J Am Chem Soc. Author manuscript; available in PMC 2019 April 18.

Published in final edited form as:

J Am Chem Soc. 2018 April 18; 140(15): 4965–4968. doi:10.1021/jacs.7b12641.

Chromophore Dipole Directs Morphology and Photocatalytic Hydrogen Generation

Adam S. Weingarten[1], **Adam J. Dannenhoffer**[2], **Roman V. Kazantsev**[1], **Hiroaki Sai**[3], **Dongxu Huang**[2], and **Samuel I. Stupp**[1,2,3,4,5,*]

[1]Department of Chemistry, Northwestern University, 2145 Sheridan Rd, Evanston, IL 60208, USA.

[2]Department of Materials Science and Engineering, Northwestern University, 2220 Campus Dr, Evanston, IL 60208, USA.

[3]Simpson Querrey Institute for Bionanotechnology, Northwestern University, 303 E. Superior St, Chicago, Illinois 60611, USA

[4]Department of Medicine, Northwestern University, 251 E. Huron St, Chicago, Illinois 60611, USA.

[5]Department of Biomedical Engineering, Northwestern University, 2145 Sheridan Rd, Evanston, Illinois 60208, USA.

Abstract

The spontaneous self-assembly of chromophores into light-harvesting antennae provides a potentially low-cost approach to building solar-to-fuel conversion materials. However, designing such supramolecular architectures requires a better understanding of the balance between non-covalent forces among the molecular components. We investigated here the aqueous assembly of perylene monoimide chromophore amphiphiles synthesized with different substituents in the 9-position. The molecular dipole strength decreases as the nature of the substituent is altered from electron donating to electron withdrawing. Compounds with stronger molecular dipoles, in which dipolar interactions stabilize assemblies by 10–15 kJ mol^{-1}, were found to form crystalline nanoribbons in solution. In contrast, when the molecular dipole moment is small, nanofibers were obtained. Highly blue-shifted absorbance maxima were observed in assemblies with large dipoles, indicating strong electronic coupling is present. However, only the moderate dipole compound had the appropriate molecular packing to access charge-transfer excitons leading to enhanced photocatalytic H_2 production.

Graphical Abstract

*Corresponding Author s-stupp@northwestern.edu.

ASSOCIATED CONTENT

Supporting Information

Synthesis, characterization, experimental methods, and supplementary figures. This material is available free of charge via the Internet at http://pubs.acs.org.

AUTHOR INFORMATION

Notes

The authors declare no competing financial interests.

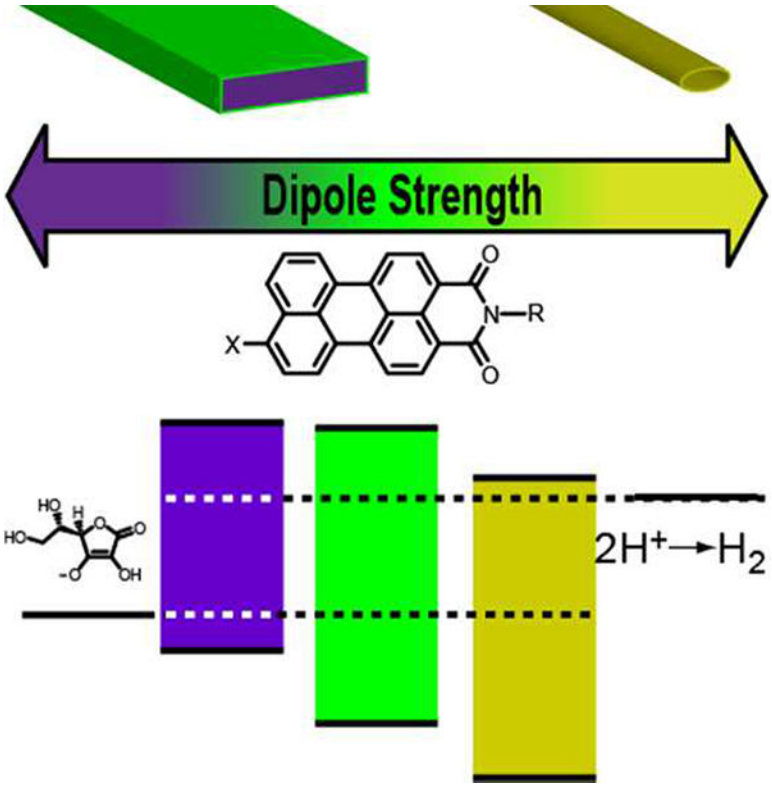

The organization of synthetic chromophores into supramolecular arrays presents an appealing approach to the construction of solar-to-fuel conversion materials.[1] Inspiration arises from natural photosynthetic machinery, in which chromophores are precisely organized into arrays that transfer energy over long distances to fuel-producing catalysts.[2] While the protein scaffold spatially positions natural chromophores, selfassembly also offers the potential to construct synthetic light harvesting arrays. In synthetic systems organization can rely on molecular design to combine extended π-π stacking for visible light absorption with hydrogen bonding,[3] van der Waals,[4] electrostatic,[5] metal-coordination[6] forces, and dipolar interactions.[7,8] The wide range of non-covalent interactions, combined with a variety of known chromophores, provides many opportunities for the design of highly functional materials.

Synthetic chromophore arrays have shown exciting advances towards a complete solar-to-fuel conversion device. Such systems enable energy or charge movement along the nanostructures across micrometer distances from the excitation site,[9] a desirable property for functional light-harvesting structures, while increasing charge carrier lifetimes can also improve charge collection.[6] Photovoltaic devices have shown power conversion efficiency enhancements using self-assembled chromophore arrays,[10,11] where device performance heavily depends on the molecular organization.[12] While solar-to-fuel conversion requires coupling light-harvesting arrays and fuel-producing catalysts, there remain few examples of photocatalysis from supramolecular chromophore arrays.[13,14] This scarcity reflects the challenge both in catalyst-chromophore integration and in understanding the design rules for beneficial solar-to-fuel molecular packing arrangements within chromophore assemblies.

We recently reported a supramolecular, light-harvesting hydrogel that photocatalytically reduces protons to H_2 in water using assemblies of chromophore amphiphiles (CAs).[15] The CAs were based on perylene monoimide (PMI), a light-absorbing molecule known for its ease of synthesis and stability, containing a carboxylate to introduce water solubility. Hydrogels could be formed through the addition of salt to aqueous solutions of self-assembled CA ribbons. Furthermore, the salt-induced charge screening resulted in crystallization, enabling us to determine intra-ribbon CA molecular packing, and increased electronic coupling between chromophores. This material's crystalline nature, a rare phenomenon for supramolecular assemblies, provides a handle to relate molecular packing, electronic properties, and photocatalytic performance. We recently altered the molecular packing arrangements within assemblies by varying the CA linker length[16] or modifying the aromatic core[17,18] and found these differences have drastic consequences on photocatalytic performance. Analyses investigating inter-chromophore electronic coupling revealed the formation of weakly bound charge-transfer exciton (CT-exciton) states to be vital for achieving the most active solar-to-fuel photosensitizing assemblies.[19] While control over self-assembly via molecular shapes appears crucial for developing future supramolecular materials, it remains uncertain how individual CA's molecular electronic properties alter assembly and photocatalytic performance.

We synthesized a series of CAs in which an electron-donating amine, an electron-neutral methyl, or an electron-withdrawing nitrile was attached to the 9-position of PMI's aromatic core (Figure 1). 9-position substitutions usually alter the core's electronic properties, such as band gap, HOMO-LUMO levels, and dipole strength.[20] The molecules, containing a hydrophilic carboxylate through the imide position, were prepared from a brominated PMI precursor using various palladium-catalyzed chemistries (see SI). We calculated dipole moments for **NH2-CA, CH_3-CA**, and **CN-CA** to be 10.2 D, 8.1 D, and 1.6 D, respectively (see SI). We also found unsubstituted PMI's dipole strength to be 7.1 D, in agreement with previous calculations.[21] **NH_2-CA**'s strong molecular dipole is consistent with π-donation by the amine nitrogen's lone pair, while **CN-CA**'s weak dipole results from competition for electron density between the electron-withdrawing nitrile and imide groups. **CH_3-CA**'s weakly-donating methyl group enhances the core dipole relative to unsubstituted PMI. Our calculations showed a decreasing trend in molecular dipole strength as the 9-position's electron-withdrawing nature is increased,[22,23] demonstrating our ability to control CA dipole strength via substituent choice.

Small angle X-ray scattering (SAXS) showed the CAs all selfassemble into nanostructures upon suspension in water (Figure 2a). **NH_2-CA** and **CH_3-CA** profiles were consistent with scattering from ribbon-like nanostructures while **CN-CA** data was best modeled by cylindrical fibers (Figure S1 and Table S1). Our models suggested that all the nanostructures are less than 5 nm thick and at least hundreds of nanometers long. However, while both **NH_2-CA** and **CH_3-CA** formed ribbons roughly 100 nm in width, **CN-CA** assembled into thin fibers, 5–10 nm wide based on SAXS fitting and cryogenic transmission electron microscopy (Figure S2). Given the similar molecular shape between the three CAs and the drastically different observed morphologies, we hypothesize that either the molecular packing differs greatly or that weakening the CA core's ground state dipole alters

supramolecular assembly. To probe the internal structure of the assemblies, we employed wide-angle X-ray scattering (WAXS) after chargescreening with salt. **NH_2-CA** and **CH_3-CA** samples showed sharp diffraction peaks, indicative of nanostructure crystallization (Figure 2b), while the broader peaks for **CN-CA** indicate organization into smaller domain sizes than the other CAs, possibly resulting from the narrow nanoribbon widths and a high degree of crystal distortions. We fit the three observed WAXS peak positions for each CA to 2D oblique lattices (Figure S3). The b-axis distances were 3.7–3.9 A, similar to π-π stacking distances reported for crystalline perylene diimide (PDI) compounds, usually 3.3–3.5 A.[24] We observed longer b-axis distances for **NH_2-CA** and **CN-CA** than **CH_3-CA**, suggesting less stable π-π stacking interactions for these two CA assemblies. We observed 7.8–8.6 A a-axis distances, possibly representing edge-to-edge or edge-to-face (herringbone) configurations. While the X-ray data lacks the fine structure necessary to determine CA orientation within these unit cells, a “herringbone” type packing is likely, given stabilization by CH-π interactions[25] and previous examples found in solid state[26] and supramolecular assemblies.[17]

We further investigated how the CA ground-state dipoles could affect nanostructure formation. Using the calculated molecular dipole strengths and CA molecular packing geometries, we estimated dipolar interaction energies among CAs (see SI and Figure S4) using a pairwise dipole-dipole interaction potential, not considering other intermolecular interactions such as van der Waals, solvophobic, π-π stacking, or CH-π stabilization forces. Interestingly, we calculated **NH_2-CA** and **CH_3-CA** to have total dipolar interaction energies of 14.5 kJ-mol^{-1} and 10.1 kJ-mol^{-1}, respectively. To compare these values with PMI’s π-π stacking energy, we conducted a classical molecular dynamics (MD) simulation, using GROMACS package,[27] for CA packing in an aqueous, charge screened medium (Figure S5). The simulations estimated the unsubstituted PMI π-π stacking energy to be 42 kJ-mol^{-1}, in accordance with previous estimates of 45 kJ-mol^{-1} for aqueous PDI π-π stacking.[28] Our calculated dipole interaction energies are well within the range of previously reported dipole-mediated aromatic assemblies,[29,30] and are similar in magnitude to π-π stacking energy, albeit several times weaker. In contrast, we calculated **CN-CA’s** dipolar interactions to provide less than 0.5 kJ-mol^{-1} stabilization, indicating that the loss of this dipole-induced stabilization could justify the narrow nanostructures observed for **CN-CA**. We propose CA dipole strength enables nanoribbon formation through dipole-dipole interactions and is a fundamental design rule to crystalline nanostructure formation. The 9-substituent should also alter CA π-basicity and therefore CH-π interactions. **CN-CA’s** nitrile reduces the CA’s π-basicity, weakening any CH-π stabilization and limiting growth perpendicular along the π-π stacking direction.

We investigated the CA assemblies using absorption spectroscopy to understand the electronic coupling within each assembly. In dimethyl sulfoxide (Figure 3a), **NH_2-CA** and **CH_3-CA** displayed featureless absorption spectra, while **CN-CA** showed the vibrational modes associated with monomeric PMI. In the presence of salt (50 mM aqueous NaCl) to screen assemblies, **NH_2-CA** solutions presented a 500 nm absorption maximum, a 115 nm blue-shift relative to the monomer spectrum (Figure 3b). **CH_3-CA** showed a 440 nm absorbance maximum and a 570 nm peak. The 570 nm peak is consistent with CT exciton

formation, which has been previously reported at 564 nm in PDI crystals.[31] **CN-CA** exhibited a 460 nm absorbance maximum, a 40 nm blue-shift from the monomer spectrum, indicating significant electronic coupling despite the broader WAXS peaks, consistent with aggregation, but not necessarily crystallization. All CAs exhibited absorbance maxima blue-shifts compared to their unassembled states, indicative of cofacial, **π-π** stacking among PMI cores (H-aggregation),[32] congruous with our proposed packing pattern. However, only **CH_3-CA** displayed evidence for CT-exciton formation, a feature we associate with improved photocatalytic performance.

We explored how CA molecular packing and electronic properties affect the CA's ability to photosensitize a proton reduction catalyst. Photocatalytic proton reduction studies were performed on CA gels (9.57 mM), produced from charge screening with PDDA (5 wt%), and placing gels in a solution of 0.85 M pH 4 ascorbate buffer and 4.3 μM $(NH_4)_2Mo_3S_{13}$ clusters, previously shown to be efficient and robust proton reduction catalysts.[33] After illuminating for 18 hours, we observed an average of 275 ± 56 turnovers or 98 ± 14 gmol H_2 g^{-1} h^{-1} for **NH_2-CA** and 478 ± 63 or 160 ± 21 μmol H_2 g^{-1} h^{-1} for **CH_3-CA**. The external quantum efficiency of our best system (**CH_3-CA**) was measured to be 0.023 ± 0.0005%, slightly lower than other high performing organic systems based on C_3N_4 and MoS_2.[34] The **CN-CA** gels did not produce any H2, and all gels experienced minimal morphological changes during the photocatalytic experiments (Figure S6). We hypothesized the absence of H2 from **CN-CA** may result from the highly electron-withdrawing nitrile group that lowers **CN-CA**'s HOMO and LUMO levels, bringing them closer to those of unsubstituted PDI[35] and too low for Mo_3S_{13} cluster photoreduction. We used cyclic voltammetry (CV) to probe energy levels of self-assembled CAs in dried films, which largely retain the gelled-state structures (Figure S7, S8, and Table S3). Our estimations suggest all three CA assemblies should be capable of photooxidizing ascorbic acid (Figure 4), but only **NH**2-**CA** and **CH_3-CA** can photoreduce Mo_3S_{13} clusters, consistent with the significant H2 evolution observed for those gels. The top of **CN-CA**'s conduction band is only 0.1 eV above the $(NH_4)_2Mo_3S_{13}$ clusters' LUMO, suggesting that photocatalysis may require a LUMO offset, comparable to the 0.3 eV required for exciton splitting in organic photovoltaic systems.[36,37] We envision the photocatalytic mechanism to proceed via CA light-induced exciton formation, followed by electron transfer from ascorbate to CA. Photoreduced **NH**2-**CA** or **CH**3-**CA** then transfers an electron to a nearby Mo_3S_{13} catalyst. A second light-induced electron transfer event results in the evolution of one H_2 molecule. As **CN-CA** cannot reduce Mo_3S_{13}, photoexcitational energy is lost via recombination instead.

CH3-**CA** produced more H2 even though its absorbance peak has less overlap with the lamp emission compared to that of **NH_2-CA** (Figure S9). We attribute **CH_3-CA**'s improved activity to its higher propensity to access CT excitons via its unique molecular packing.[19] Furthermore, the formation of a CT state, in which excitation energy is shared across adjacent CAs, may "pre-split" the exciton to improve electron or hole transfer. We observed no evidence for low-energy excimer formation (Figure S10).[32] Therefore, the CT exciton is likely the lowest energy excited state and hence the most relevant for photochemical processes. While the **CN-CA** does not appear to form CT states, its inability to sensitize H_2 evolution likely results from its LUMO energy being too low to transfer an electron to the

catalyst. We conclude both well-positioned energy levels and molecular organization are necessary to maximize the photocatalytic performance of supramolecular materials.

In conclusion, we demonstrated the electronic properties of the CA molecules profoundly impact both assembly morphology and H2 photocatalysis. CAs with strong molecular dipoles crystallized into nanoribbons while CAs with a weak molecular dipole assembled into non-crystalline nanofibers. The strong ground state dipoles introduce 10–15 kJ/mol stabilization to the ribbon shaped nanostructures, possibly explaining why these CAs crystallize within assemblies while many other self-assembling chromophore systems do not. Dipole-dipole interactions thus represent an important design criterion for understanding how tailoring chemical structure modifies the molecular packing and controls lightharvesting functionality of self-assembled architectures, a unique aspect of the supramolecular materials.

Supplementary Material

Refer to Web version on PubMed Central for supplementary material.

ACKNOWLEDGMENTS

This work was supported as part of the Argonne-Northwestern Solar Energy Research (ANSER) Center, an Energy Frontier Research Center funded by the U.S. Department of Energy, Office of Science, Basic Energy Sciences under Award # DE-SC0001059. Use of the Advanced Photon Source (APS) was supported by the U.S. Department of Energy, Office of Science, Basic Energy Sciences, under Contract No. DE-AC02–06CH11357. SAXS experiments were performed at the DuPont-Northwestern-Dow Collaborative Access Team (DND-CAT) located at Sector 5 of APS.DND-CAT is supported by E.I. DuPont de Nemours & Co., The Dow Chemical Company and Northwestern University. WAXS experiments were conducted BioCARS Sector 14 at the APS was supported by grants from the National Center for Research Resources (5P41RR007707) and the National Institute of General Medical Sciences (8P41GM103543) from the National Institutes of Health. GIXS data was collected at Sector 8-ID-E of APS. We thank the Biological Imaging Facility (BIF) at Northwestern for the use of TEM equipment and Electron Probe Instrumentation Center (EPIC) facilities of the Northwestern University Atomic and Nanoscale Characterization Experimental (NUANCE) which has received support from the MRSEC program (NSF DMR-1121262) at the Materials Research Center; the Nanoscale Science and Engineering Center (NSF EEC-0647560) at the International Institute for Nanotechnology; and the State of Illinois, through the International Institute for Nanotechnology, for the use of SEM equipment. NMR and MS equipment at the Integrated Molecular Structure Education and Research Center (IMSERC) was supported by the National Science Foundation under CHE-9871268. We would also like to thank Dr. Liam Palmer for helpful support and feedback.

REFERENCES

(1). Wasielewski MR Acc. Chem. Res 2009, 42, 1910.19803479

(2). Amunts A ; Toporik H ; Borovikova A ; Nelson NJ Biol. Chem 2010, 285, 3478.

(3). Korevaar PA ; George SJ ; Markvoort AJ ; Smulders MMJ ; Hilbers PAJ ; Schenning APHJ ; De Greef TFA ; Meijer EW Nature 2012, 481, 492.22258506

(4). Krieg E ; Shirman E ; Weissman H ; Shimoni E ; Wolf SG ; Pinkas I ; Rybtchinski BJ Am. Chem. Soc 2009, 131, 14365.

(5). Liu K ; Xing R ; Chen C ; Shen G ; Yan L ; Zou Q ; Ma G ; Mohwald H ; Yan X Angew. Chem. Int. Ed 2015, 54, 500.

(6). Zhang W ; Jin W ; Fukushima T ; Saeki A ; Seki S ; Aida T Science 2011, 334, 340.22021852

(7). Foster EJ ; Jones RB ; Lavigueur C ; Williams VE J. Am. Chem. Soc 2006, 128, 8569.16802823

(8). Chen L ; Dou X ; Pisula W ; Yang X ; Wu D ; Floudas G ; Feng X ; Mullen K Chem. Commun 2012, 48, 702.

(9). Haedler AT ; Kreger K ; Issac A ; Wittmann B ; Kivala M ; Hammer N ; Kohler J ; Schmidt H-W ; Hildner R Nature 2015, 523, 196.26156373

(10). Lee OP ; Yiu AT ; Beaujuge PM ; Woo CH ; Holcombe TW ; Millstone JE ; Douglas JD ; Chen MS ; Frechet JM J. Adv. Mater 2011, 23, 5359.

(11). Ruiz-Carretero A ; Aytun T ; Bruns CJ ; Newcomb CJ ; Tsai W-W ; Stupp SI J. Mater. Chem. A 2013, 1, 11674.

(12). Aytun T ; Barreda L ; Ruiz-Carretero A ; Lehrman JA ; Stupp SI Chem. Mat 2015, 27, 1201.

(13). Chen S ; Jacobs DL ; Xu J ; Li Y ; Wang C ; Zang L RSC Adv. 2014, 4, 48486.

(14). Liu D ; Wang J ; Bai X ; Zong R ; Zhu Y Adv. Mater 2016, 28, 7284.27311128

(15). Weingarten AS ; Kazantsev RV ; Palmer LC ; McClendon M ; Koltonow AR ; Samuel APS ; Kiebala DJ ; Wasielewski MR ; Stupp SI Nat. Chem 2014, 6, 964.25343600

(16). Weingarten AS ; Kazantsev RV ; Palmer LC ; Fairfield DJ ; Koltonow AR ; Stupp SI J. Am. Chem. Soc 2015, 137, 15241.26593389

(17). Harutyunyan B ; Dannenhoffer A ; Kewalramani S ; Aytun T ; Fairfield DJ ; Stupp SI ; Bedzyk MJ J. Phys. Chem. C 2017, 121, 1047.

(18). Kazantsev RV ; Dannenhoffer AJ ; Weingarten AS ; Phelan BT ; Harutyunyan B ; Aytun T ; Narayanan A ; Fairfield DJ ; Boekhoven J ; Sai H ; Senesi A ; O'Dogherty PI ; Palmer LC ; Bedzyk MJ ; Wasielewski MR ; Stupp SI J. Am. Chem. Soc 2017, 139, 6120.28436654

(19). Hestand NJ ; Kazantsev RV ; Weingarten AS ; Palmer LC ; Stupp SI ; Spano FC J. Am. Chem. Soc 2016, 138, 11762.27589150

(20). Roznyatovskiy VV ; Gardner DM ; Eaton SW ; Wasielewski MR Org Lett 2014, 16, 696.24417249

(21). Lefler KM ; Co DT ; Wasielewski MR J. Phys. Chem. Lett 2012, 3, 3798.26291113

(22). Hammett LP J. Am. Chem. Soc 1937, 59, 96.

(23). Hansch C ; Leo A ; Taft RW Chem. Rev 1991, 91, 165.

(24). Hartnett PE ; Timalsina A ; Matte HSSR ; Zhou N ; Guo X ; Zhao W ; Facchetti A ; Chang RPH ; Hersam MC ; Wasielewski MR ; Marks TJ J. Am. Chem. Soc 2014, 136, 16345.25350908

(25). Guijarro A ; Verges JA ; San-Fabian E ; Chiappe G ; Louis E ChemPhysChem 2016, 17, 3548.27653622

(26). Schmidt R ; Oh JH ; Sun Y-S ; Deppisch M ; Krause A-M ; Radacki K ; Braunschweig H ; Konemann M ; Erk P ; Bao Z ; Wurthner FJ Am. Chem. Soc 2009, 131, 6215.

(27). Caleman C ; van Maaren PJ ; Hong M ; Hub JS ; Costa LT ; van der Spoel DJ Chem. Theory Comput 2012, 8, 61.

(28). Chen Z ; Fimmel B ; Wurthner F Org. Biomol. Chem 2012, 10, 5845.22391667

(29). Jiang J ; Lima OV ; Pei Y ; Zeng XC ; Tan L ; Forsythe EJ Am. Chem. Soc 2009, 131, 900.

(30). Haase N ; Grigoriadis C ; Butt H-J ; Mullen K ; Floudas GJ Phys. Chem. B 2011, 115, 5807.

(31). Gisslen L ; Scholz R Phys. Rev. B: Condens. Matter 2009, 80, 115309.

(32). Lindquist RJ ; Lefler KM ; Brown KE ; Dyar SM ; Margulies EA ; Young RM ; Wasielewski MR J. Am. Chem. Soc 2014, 136, 14912.25245598

(33). Kibsgaard J ; Jaramillo TF ; Besenbacher F Nat. Chem 2014, 6, 248.24557141

(34). Xu H ; Yi J ; She X ; Liu Q ; Song L ; Chen S ; Yang Y ; Song Y ; Vajtai R ; Lou J ; Li H ; Yuan S ; Wu J ; Ajayan PM Appl. Catal., B 2018, 220, 379.

(35). Bullock JE ; Vagnini MT ; Ramanan C ; Co DT ; Wilson TM ; Dicke JW ; Marks TJ ; Wasielewski MR J. Phys. Chem. B 2010, 114, 1794.20073517

(36). Thompson BC ; Frechet JM J. Angew. Chem. Int. Ed 2008, 47, 58.

(37). Heeger AJ Adv. Mater 2014, 26, 10.24311015

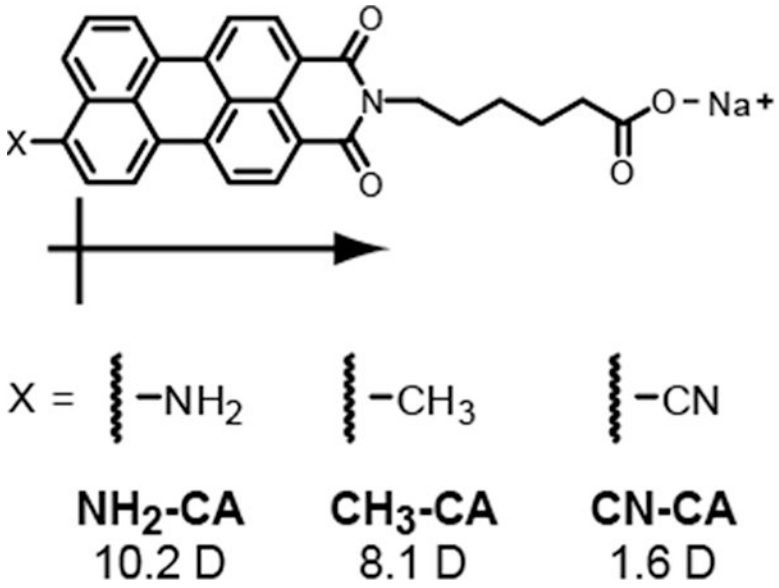

Figure 1.
Chemical structure of CAs and dipole strengths calculated from density functional theory simulation.

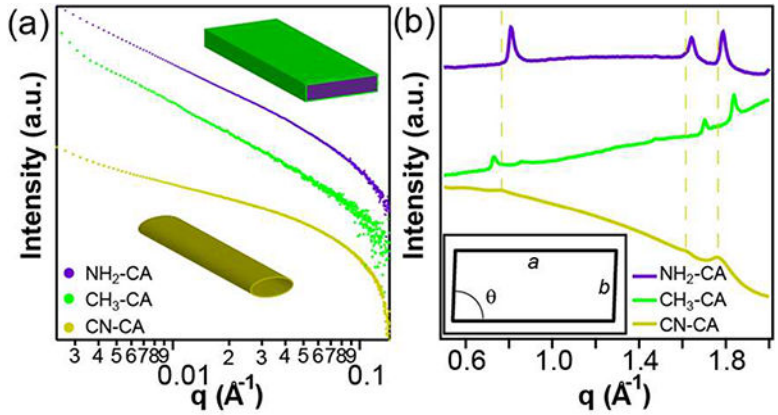

Figure 2.

X-ray scattering data for CA series. (a) SAXS patterns for 9.57 mM aqueous CA solutions in 50 mM NaCl. **NH_2-CA** and **CH_3-CA** data correspond to a ribbon morphology, while the **CN-CA** scattering is best fit to a fibrous morphology. (b) WAXS data for CAs gelled with PDDA. The three visible diffraction peaks imply diffraction by a 2D oblique lattice unit cell (inset).

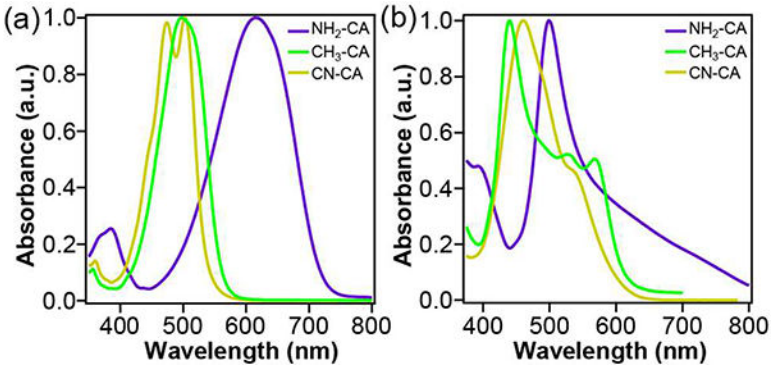

Figure 3.

Absorption spectra of CAs in (a) 1:9 DMSO/H_2O at 1.15 mM and (b) in 50 mM aqueous NaCl at 9.57 mM.

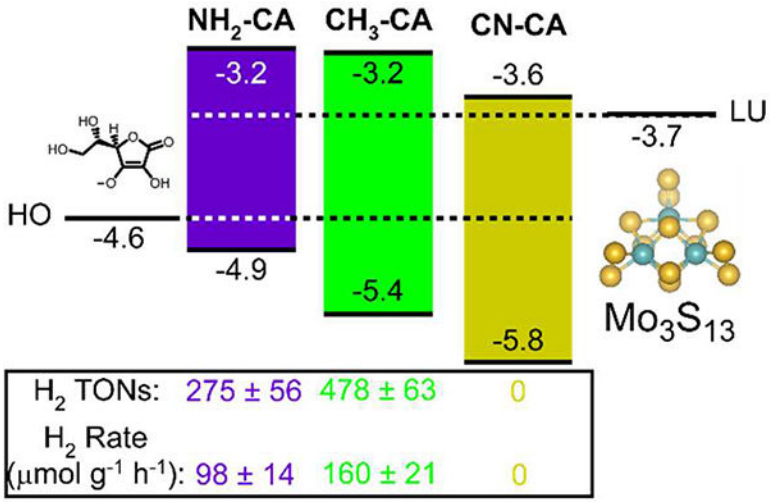

Figure 4.

Energy level diagram of CAs calculated from CV and absorption spectra, against vacuum, with oxidation and reduction potentials of ascorbate and Mo_3S_{13}, respectively. Values are given in electron-volts (eV).